






Article

Predefined-Time Fractional-Order Tracking Control for UAVs with Perturbation

Abdellah Benaddy ¹, Moussa Labbadi ^{2,*}, Sahbi Boubaker ^{3,*}, Faisal S. Alsubaei ⁴ and Mostafa Bouzi ¹

¹ MIET Laboratory, Faculty of Science and Technology, Hassan First University of Settat, Settat 26000, Morocco; a.benaddy@uhp.ac.ma (A.B.); mostafa.bouzi@uhp.ac.ma (M.B.)

² LIS UMR CNRS 7020, Aix-Marseille University, 13013 Marseille, France

³ Department of Computer & Network Engineering, College of Computer Science and Engineering, University of Jeddah, Jeddah 21959, Saudi Arabia

⁴ Department of Cybersecurity, College of Computer Science and Engineering, University of Jeddah, Jeddah 23218, Saudi Arabia; fsalsubaei@uj.edu.sa

* Correspondence: moussa.labbadi@lis-lab.fr (M.L.); sboubaker@uj.edu.sa (S.B.)

Abstract: This manuscript describes the design of a controller that assures predefined-time convergence in fractional-order sliding mode control (PTFOSMC) for a quadrotor UAV subjected to matched perturbation. Moreover, predefined-time techniques enable the establishment of a time constraint for convergence as a control parameter, distinguishing them from finite- and fixed-time controllers. The proposed control offers the advantage of sliding mode control, exhibiting rapid response and robust performance for the quadrotor subsystems. Notably, the suggested controller is devoid of terms dependent on the initial conditions of the quadrotor. Additionally, an established switching-type predefined-time controller with fractional-order is introduced to bolster robustness against external disturbances and alleviate the chattering problem associated with the sliding mode technique. The application of the Lyapunov function is employed to analyze the predefined-time stability of the quadrotor utilizing the suggested PTFOSMC. Numerical results are provided to demonstrate the effectiveness of the suggested scheme.

Keywords: quadrotor UAV; predefined-time stability; fractional order; sliding mode control; Lyapunov function; external disturbances

MSC: 93D30; 93-11



Citation: Benaddy, A.; Labbadi, M.; Boubaker, S.; Bouzi, M. Predefined-Time Fractional-Order Tracking Control for UAVs with Perturbation. *Mathematics* **2023**, *11*, 4886. <https://doi.org/10.3390/math11244886>

Academic Editors: Mihail Ioan Abrudean and Vlad Muresan

Received: 8 November 2023

Revised: 2 December 2023

Accepted: 4 December 2023

Published: 6 December 2023



Copyright: © 2023 by the authors. Licensee MDPI, Basel, Switzerland. This article is an open access article distributed under the terms and conditions of the Creative Commons Attribution (CC BY) license (<https://creativecommons.org/licenses/by/4.0/>).

1. Introduction

1.1. Motivations and Background

Quadrotors have grown in popularity in recent years as a result of rapid technical advancement, which has had a considerable impact on current electronic components, such as microcontrollers, sensors, and low-cost development. These advancements work in favor of this platform, propelling it to mainstream status. Many researchers have tackled the topic of trajectory tracking of quadrotor systems in the past decade due to the numerous applications of this vehicle [1,2], including military, highway monitoring [3], photography and videography, geographic mapping of inaccessible terrain and locations, delivery systems [4], surveillance [5], detection, scientific research and development, identification of different objects, search and rescue missions [6], and agriculture. The dynamics of the quadrotor system in real flight involve parameter uncertainty and external disturbances, which negatively impact stabilization and tracking performance. Different control methods have been developed to address these challenges, particularly sliding mode control (SMC) and advanced control systems based on SMC, such as nonsingular fast terminal SMC [7], fixed-time distributed robust SMC [8], adaptive backstepping fast terminal SMC [9], developing PID in sliding mode controllers [10], etc.

1.2. Related Works

One of the most challenging aspects of UAVs is achieving smooth, precise flight. To attain this, optimal, stable controllers must be implemented under external disturbances. A literature review will be offered in this subsection. An investigation of sliding mode controllers in predefined time is suggested by the authors in [11]. They conducted a comparison analysis that emphasized the benefits and drawbacks of each technique used for the flight controller to drive a quadrotor. According to the findings of the comparison analysis, the fractional-order integral terminal sliding-mode control method was chosen as the optimal solution for a quadrotor system. The quadrotor model was obtained using the Lagrange-Euler approach in [12]. To adhere to the position trajectory, a predictive control approach with integral action is formulated, and H^∞ control is devised to stabilize the orientation of the quadrotor. The researchers in [13] offer a robust control strategy based on a second-order SMC approach to improve quadrotor position tracking performance. In [14], the external disturbances and unknown states of the quadrotor are calculated using an observer. This is done to estimate the total disturbances and control the quadrotor. The controller and observer are designed in the attitude and position subsystems. An observer is formed to assess outside disturbances and unknown situations. The TSMC is intended to provide finite-time convergence performance through composite learning, neural approximation, and disturbance estimation [15].

The current study provides a FO hybrid finite-time control strategy with fractional-order dynamics to address the trajectory tracking of quadrotors, motivated by previous research and inspired by Reference [16]. The quadrotor system, benefiting from fixed-time stability, can achieve convergence to a stable range within a specified upper-bound convergence time, independent of the initial operational states [17]. As a result, the authors in ref. [18] introduces distributed fixed-time control methods to enhance the performance of power systems. On the flip side, the fixed-time control approach exhibits superior capabilities in surmounting these limitations. Nevertheless, estimating the convergence time of the nonlinear system under the fixed-time control approach is not straightforward; it requires the use of a sophisticated estimation function grounded in tuning parameters [19]. Predefined-time stability can keep the nonlinear system stable within a predetermined upper limited convergence time, which is directly associated with an adjustable variable [20,21]. Although less conservative than the fixed-time control approaches now in use, the system's upper limited convergence time under predefined-time control methods is still adequate [22,23]. The fixed-time control method and the finite-time control method have drawbacks, which can be more effectively addressed by the predefined-time control strategy. Fractional-order integral/derivative operators have been extensively used in research on the control of engineering systems. A fractional-order error manifold for robot manipulators was developed in [24] to achieve good performances and a more flexible PID controller structure.

In general, sliding-mode control stands out as a potent nonlinear control strategy employing discontinuous control to steer system state trajectories onto a predefined sliding surface. Its straightforward implementation and advantageous resilience characteristics make the SMC approach a popular choice, particularly for its robustness against model parameter uncertainty and external disturbances. Indeed, the effectiveness of this approach, a quality relatively rare among nonlinear design strategies, has spurred the exploration of various new research avenues within the broader field of sliding mode control. The majority of current SMC methods utilize a linear sliding mode surface, leading the system state variables to converge asymptotically or exponentially to the origin within a finite time [14]. To address this problem, terminal SMC was introduced to ensure finite-time stability [7,11]. A hybrid finite-time control technique based on nonsingular terminal SMC and adaptive integral SMC approaches is provided to handle quadrotor path tracking problems with unknown dynamics and disturbances in [25]. The initial conditions of the state variables adversely affect the achieved finite time, with this impact intensifying as the values of these initial states increase. Recent endeavors in this domain have focused on fixed-time

stability [17,19]. On the flip side, the settling time holds significance in the trajectory tracking of the quadrotor system. Consequently, a novel concept called predefined-time stability has emerged to enhance state convergence [19,20,22]. Moreover, the aim is to showcase the efficacy and superior performance of the proposed control for the quadrotor system in comparison to existing control methods. Subsequently, communication network and load changes are integrated into simulations using the Matlab/Simulink platform.

1.3. Contributions

Inspired by the works described in the related works subsection and guided by the paper in [26], a novel predefined-time fractional-order sliding mode controller (PTFOSMC) method based on fractional calculus, SMC, and predefined-time stability is suggested to improve the dynamic performance of the quadrotor. The current study examines the disturbances and variations in the drag coefficients of rotational and translational subsystems. The proposed PTFOSMC ensures that the quadrotor system will converge to a stable zone with specified performance within the predetermined time. In comparison with standard SMC [9,10], the PTFOSMC may offer better results, such as faster convergence speed, reduced overshoot, lower error, and lower chattering impact. The contributions of this research can be encapsulated in the following key points:

- The proposed method completes the stabilization and optimization procedures within a predefined time.
- The predefined-time fractional-order sliding mode control exhibits minimal overshoot, the smallest error, and faster variable convergence.
- Utilizing the proposed control, the stability of the quadrotor system within a predefined time is assessed through the application of the Lyapunov function. Simulations are employed to validate the efficacy of the suggested control for the quadrotor system.
- The simulation results show that, in comparison to current flight controllers, the suggested controller enables the quadrotor to achieve the intended flight trajectory with high accuracy.

2. Preliminary Knowledge

2.1. Predefined-Time Stability

The subsequent section revisits the predefined-time stability of integer-order systems. We examine the characteristics of the integer-order system.

$$\dot{x} = g_1(t, x) \quad (1)$$

where $x \in \mathbb{R}^n$ represents the system state. Function $g_1 : \mathbb{R}_+ \times \mathbb{R}^n \mapsto \mathbb{R}^n$ is nonlinear, and if we consider the origin as an equilibrium point, then $g_1(t, 0) = 0$. The initial condition is $x_0 = x(0)$. The subsequent definitions bear particular significance.

Definition 1 (Globally finite-time design [27]). *Any solution $x(t)$ of (1) converges to the origin at some finite time, and the origin of (1) is asymptotically stable; that is, $x(t) = 0 \forall t \geq T(x(0))$, where $T : \mathbb{R}^n \rightarrow \mathbb{R}_{\geq 0}$ is the function of the settling time.*

Definition 2 (Globally fixed-time design [28]). *If the settling-time function is bounded and the origin of system (1) is finite-time stable, then the basis is fixed-time stable, i.e., $\exists T_{\max} > 0 : T(x(0)) \leq T_{\max}, \forall x(0) \in \mathbb{R}^n$.*

Definition 3 (Settling-time design [29]). *Let the set of all settling-time function bounds for system (1) be written above:*

$$\mathcal{T} = \{T_{\max} \in \mathbb{R}_+ : T(x_0) \leq T_{\max}\}. \quad (2)$$

Furthermore, the ensuing definitions elucidate the design centered on prescribed-time stability and the design rooted in prescribed-time stability.

Definition 4 (Prescribed-time design [29]). Take the \mathcal{T} set given in (2). In the specific instance for system (1), T_{max} can be modified by a specific selection of system parameters, ρ , $T_{max} = T_{max}(\rho)$, referred to the concept of prescribed-time stability. This design is accomplished by selecting $T_{max}(\rho) \in \mathcal{T}$ and finding the inverse of the settling-time function, allowing for modifying ρ .

Remark 1. It is crucial to emphasize that the precise fixed stabilization time for a system built upon prescribed-time stability remains unknown but is confined within $T_{max}(\rho)$. In contrast, a design system employing predefined-time stability features a known stabilization time.

Definition 5 (Predefined-time design [30]). For a predefined-time constant, $T_c > 0$, the origin of system (1) is predefined-time stable if it is fixed-time stable and the settling-time function is fulfilled.

$$T(x(0)) \leq T_c, \quad \forall x(0) \in \mathbb{R}^n,$$

where T_c is signified by a predefined time.

2.2. Fractional-Order Calculus

The differentiation and integration of fractional order are studied in fractional calculus. The following operators are defined [31,32].

Definition 6. The following definition applies to the function $f(t)$ using the Riemann–Liouville fractional derivative order α [31]:

$${}^{\text{RL}}D_t^\alpha f(t) = \frac{1}{\Gamma(m - \alpha)} \frac{d^m}{dt^m} \int_a^t \frac{f(\tau)}{(t - \tau)^{\alpha - m + 1}} d\tau$$

where $\Gamma(\cdot)$ is the Gamma function and $(m - 1) < \alpha \leq m$.

Definition 7. The definition of the fractional-order derivative, as introduced by Caputo for a function $f(t)$, can be expressed as follows [31]:

$${}^{\text{C}}D_t^\alpha f(t) = \frac{1}{\Gamma(m - \alpha)} \int_a^t \frac{f^m(\tau)}{(t - \tau)^{\alpha - m + 1}} d\tau, \quad (m - 1) < \alpha < m$$

with $m \in \mathbb{N}^*$ and $\alpha \in \mathbb{R}^+$.

Property 1. The Caputo derivative is the equivalent of the following equality [32].

$${}^{\text{C}}D_t^\alpha \left({}^{\text{C}}D_t^{-\beta} f(t) \right) = {}^{\text{C}}D_t^{\alpha - \beta} f(t) \tag{3}$$

where $\alpha > \beta > 0$

Property 2. If $1 > \alpha > 0$, we have the ability to write 4 the Caputo derivative [32]

$${}^{\text{C}}D_t^{1 - \alpha} \left({}^{\text{C}}D_t^\alpha f(t) \right) = {}^{\text{C}}D_t^\alpha \left({}^{\text{C}}D_t^{1 - \alpha} f(t) \right) = \dot{f}(t) \tag{4}$$

To represent the Caputo operator, ${}^{\text{C}}D^\alpha$ will be used in place of ${}^{\text{C}}D^\alpha$ throughout this paper.

Lemma 1 ([28]). Suppose the following condition can be satisfied:

$$\dot{V} \leq -\mu V^v - \zeta V^\tau, \quad V(0) = V_0$$

where V denotes a positive-definite function; $0 < \tau < 1$, $v > 1$, μ , and ζ are positive constants. The system $\dot{x} = f(x, t)$ will exhibit fixed-time stability, and the upper limit on the convergence time can be attained through

$$T \leq T_{\max} = \frac{1}{\mu(v-1)} + \frac{1}{\zeta(1-\tau)} \tag{5}$$

Lemma 2 ([22]). *If V can meet the following predefined-time stabilizing function:*

$$\dot{V} \leq -\frac{1}{\mu T_s} e^{(V^\mu)} V^{1-\mu}, \quad 0 < \mu < 1 \tag{6}$$

then $\dot{x} = f(x, t)$ will achieve predefined-time stability within a predefined time $T_s > 0$. That is, $\dot{x} = f(x, t)$ will converge to zero for $t \geq T_s$.

Remark 2. *As demonstrated in (5), the upper limited convergence time cannot be achieved explicitly because the adjustable parameters affect how the upper limited convergence time of the fixed-time stability is evaluated. The upper bound convergence time of the predefined-time stability is equal to the tuning parameter, as demonstrated in Lemma 2, eliminating the drawbacks of the fixed-time stability.*

3. Problem Formulation

The quadrotor employed in this investigation is illustrated in Figure 1. This apparatus features a sturdy body with four rotors. Yaw movement is generated by creating a speed differential between two rotors moving in opposite directions, specifically between rotors (2,4) and (1,3). Vertical displacement of the quadrotor is accomplished by adjusting the total rotor speeds. Forward motion is achieved by modifying the speeds of the (1 and 3) propellers. The lateral motion is created by varying the speed of the propellers (2 and 4). As a result, the body is intrinsically unstable, with a mechanical system that is tightly linked and under-actuated. Furthermore, the quadrotor dynamic model is developed on the following assumptions; the influence of the ground is disregarded, the quadrotor structure is symmetrical, the quadrotor frame and its blades possess rigidity, and the torques and thrust produced by the rotor speeds exhibit a proportionality to the square of the rotor rotation speeds.

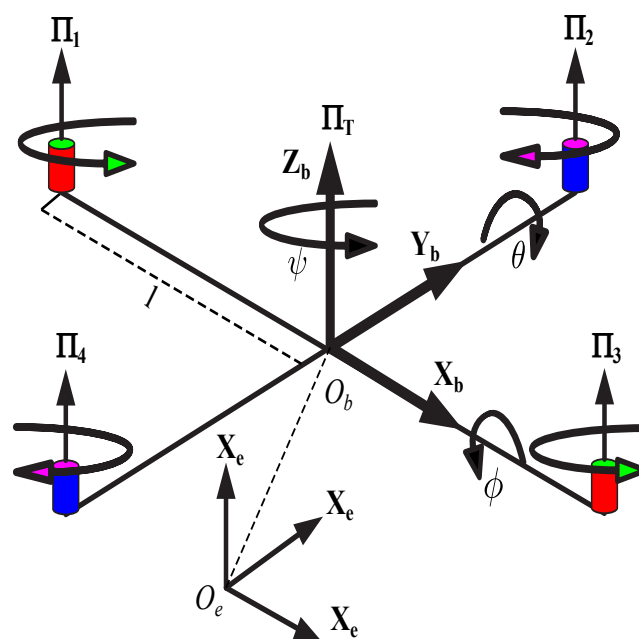


Figure 1. The four-rotor drone arrangement.

The quadrotor provides six outputs $[\phi, \theta, \psi, x, y, z]^T$ in its translational and rotational motions. Four actual voltage inputs $[(\Pi_1, \Pi_2, \Pi_3, \Pi_4)^T$ drive these outputs. The earth-fixed frame and the body frames are represented by $\mathbb{E} = [x_e, y_e, z_e]^T$ and $\mathbb{B} = [x_b, y_b, z_b]^T$,

respectively. The quadrotor dynamics can be expressed using the Newton–Euler formalism as follows [7,33].

$$\begin{cases} \ddot{\phi} = \delta_1 \dot{\theta} \dot{\psi} + \delta_2 \omega_r \dot{\theta}^2 + \delta_3 \dot{\phi} + J_x^{-1} \Pi_2 + \mathfrak{d}_\phi \\ \ddot{\theta} = \delta_4 \dot{\phi} \dot{\psi} + \delta_5 \omega_r \dot{\phi}^2 + \delta_6 \dot{\theta} + J_y^{-1} \Pi_3 + \mathfrak{d}_\theta \\ \ddot{\psi} = \delta_7 \dot{\phi} \dot{\theta} + \delta_8 \dot{\psi} + J_z^{-1} \Pi_4 + \mathfrak{d}_\psi \\ \ddot{x} = \delta_9 \dot{x} + \Pi_x + \mathfrak{d}_x \\ \ddot{y} = \delta_{10} \dot{y} + \Pi_y + \mathfrak{d}_y \\ \ddot{z} = \delta_{11} \dot{z} + \Pi_z + \mathfrak{d}_z \end{cases} \tag{7}$$

with

$$\begin{aligned} \delta_1 &= (J_y - J_z) / J_x, \delta_2 = -J_r / J_x, \delta_3 = -K_{ax} / J_x \\ \delta_4 &= (J_z - J_x) / J_y, \delta_5 = J_r / J_y, \delta_6 = -K_{ay} / J_y \\ \delta_7 &= (J_x - J_y) / J_z, \delta_8 = -K_{az} / J_z, \delta_9 = -k_x / m, \\ &\delta_{10} = -k_y / m, \delta_{11} = -k_z / m \end{aligned}$$

where m is the total body mass and g denotes gravitational acceleration. Inertia moments of the quadrotor around the x , y , and z axes are denoted by J_x , J_y , and J_z . The torques and thrusts are represented by Π_{1-4} , and $\mathfrak{d}_{x-\psi}$ represent the disturbances. The following equation represents the relation between the control signals and the rotor speeds:

$$\begin{bmatrix} \Pi_1 \\ \Pi_2 \\ \Pi_3 \\ \Pi_4 \end{bmatrix} = \begin{bmatrix} \hbar & -\hbar & \hbar & -\hbar \\ -\ell b & 0 & b \ell & 0 \\ 0 & -\ell b & 0 & b \ell \\ b & b & b & b \end{bmatrix} \begin{bmatrix} \omega_1^2 \\ \omega_2^2 \\ \omega_3^2 \\ \omega_4^2 \end{bmatrix} \tag{8}$$

where \hbar represents the drag coefficient, ω_{1-4} denotes the angular rotor speeds, b and ℓ are positive constants. The vehicle must be stabilized and follow the reference trajectory $[\phi_d, \theta_d, \psi_d, X_d, Y_d, Z_d]^T$ within a finite time. The aim of this study is to formulate a reliable controller capable of supplying thrust magnitude and torque. To streamline the approach to control system design, the following definition relates to the virtual control signals utilized to determine the overall thrust and desired angles.

$$\begin{cases} \Pi_x = (\cos(\phi) \sin(\theta) \cos(\psi) + \sin(\phi) \sin(\psi)) \frac{\Pi_1}{m} \\ \Pi_y = (\cos(\phi) \sin(\theta) \sin(\psi) - \sin(\phi) \cos(\theta)) \frac{\Pi_1}{m} \\ \Pi_z = \cos(\phi) \cos(\theta) \frac{\Pi_1}{m} - g \end{cases} \tag{9}$$

Based on the position controls, we can calculate the thrust Π_1 and the two attitude angles, ϕ_d and θ_d :

$$\begin{cases} \phi_d = \text{atan}[c(\theta_d)(\Pi_x s(\psi_d) - \Pi_y c(\psi_d)) / (\Pi_z + g)] \\ \theta_d = \text{atan}[(\Pi_x \cos(\psi_d) + \Pi_y \sin(\psi_d)) / (\Pi_z + g)] \\ \Pi_1 = m \sqrt{\Pi_x^2 + \Pi_y^2 + (\Pi_z + g)^2} \end{cases} \tag{10}$$

4. Predefined-Time Fractional-Order Controller Design

This section focuses on the design of the flight controller for the quadrotor system. Under the control of the flight controller, the closed-loop stability in the predetermined time is guaranteed, and the trajectories follow their references. The outer and inner loops now use a new predefined-time fractional-order sliding mode control, as seen in Figure 2. In comparison to the backstepping sliding mode and developing PID sliding mode controls,

the proposed control enhances the tracking capabilities of the path reference and increases the resilience control of the quadrotor against external disturbances.

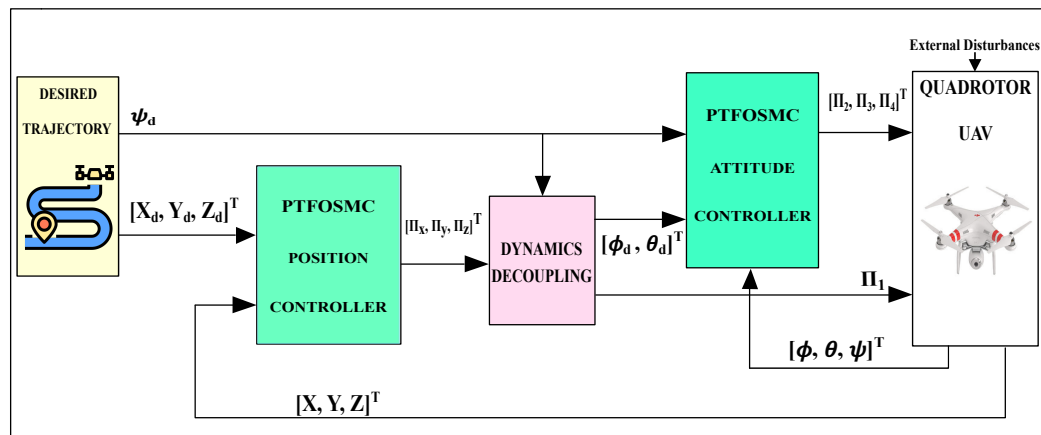


Figure 2. The proposed improved PTFOSMC method is illustrated in a block diagram.

4.1. Outer-Loop Control Design

To guarantee the predefined-time stability of the position subsystem and the generation of tilting angles, the main challenge tackled in this section involves the formulation of virtual control laws.

For the elevation subsystem, where the PTFOSMC is employed, the definition of the tracking error for the $z(t)$ subsystem and its time derivative can be established as follows:

$$\begin{cases} e_x = z - z_d \\ \dot{e}_x = \dot{z} - \dot{z}_d \end{cases} \tag{11}$$

Remark 3. The predefined-time controller ensures the convergence of the tracking error and its time derivative using the parameter T_f [34], such that

$$\lim_{t \rightarrow T_f} e_z(t) = 0, \quad \lim_{t \rightarrow T_f} \dot{e}_z(t) = 0, \\ \text{and } e_z(t) = \dot{e}_z(t) = 0 \quad t > T_f$$

The following predefined-time fractional-order sliding manifold is suggested to stabilize the altitude subsystem.

$$\sigma_z = I^{\alpha_z} \left\{ \frac{1}{T_{sz}\mu_z} e^{(|e_z|^{\mu_z})} [e_z]^{1-\mu_z} \right\} + \gamma_z D^{1-\alpha_z} e_z(t) \tag{12}$$

where e_z is the error tracking, T_{sz} denotes the predefined setting upper bound convergence time, and $[e_z(t)]^{\mu_{z2}} = |e_z| \cdot \text{sign}(e_z(t))$ with $0 < \mu_{z2} < 1$.

When the consensus error e_z reaches the fractional-order sliding surface and finds the equivalent control law, the following equations can be achieved:

$$D^\alpha \sigma_z = 0 \tag{13}$$

Assuming that, using (12) and (13), (15) can be written as

$$\frac{1}{T_{sz}\mu_z} e^{(|e_z|^{\mu_z})} [e_z]^{1-\mu_z} + \gamma_z D^1 e_z(t) = 0 \tag{14}$$

As a result, it is possible to generate the dynamics of the fractional-order sliding surface in (12), as

$$\dot{e}_z(t) = -\frac{1}{\gamma_z T_{sz}\mu_z} e^{(|e_z|^{\mu_z})} [e_z]^{1-\mu_z} \tag{15}$$

The fractional-order sliding surface σ_z will converge to zero if the dynamic system in (15) is stable.

Theorem 1. Consider the PTFO sliding manifold designed in (12); the convergence to zero in a predefined time T_{sz} of the dynamics system defined in (7) is ensured.

Proof. The function is chosen to confirm the system’s stability. Function (16) is chosen to ensure the stability of the z-subsystem:

$$V_{1z} = |e_z| \tag{16}$$

The time differentiation of V_{1z} is achieved as follows:

$$\begin{aligned} \dot{V}_{1z} &= \text{sign}(e_z)\dot{e}_z = \text{sign}(e_z)D^\alpha D^{1-\alpha}e_z \\ &= \text{sign}(e_z)D^\alpha \left(-D^{-\alpha_z} \frac{1}{\gamma_z T_{sz} \mu_z} e^{(|e_z|^{\mu_z})} [e_z]^{1-\mu_z} \right) \\ &= \text{sign}(e_z) \left(-\frac{1}{\gamma_z T_{sz} \mu_z} e^{(|e_z|^{\mu_z})} [e_z]^{1-\mu_z} \right) \end{aligned} \tag{17}$$

Due to $\text{sign}(e_z) \times \text{sign}(e_z) = 1$, (18) can be achieved as follows:

$$\begin{aligned} \dot{V}_{z1} &= \text{sign}(e_i) \left(-\frac{1}{\gamma_z T_{sz} \mu_z} e^{(|e_z|^{\mu_z})} \text{sign}(e_i) |e_z|^{1-\mu_z} \right) \\ &= -\frac{1}{\gamma_z T_{sz} \mu_z} e^{(|e_z|^{\mu_z})} |e_z|^{1-\mu_z} \\ &= -\frac{1}{\gamma_z T_{sz} \mu_z} e^{(|V_{1z}|^{\mu_z})} |V_{1z}|^{1-\mu_z} \leq 0 \end{aligned} \tag{18}$$

□

Based on Lemma 2, it is shown that the dynamic system described by (18) can achieve convergence to zero within a predefined time T_{sz} . In order to prove this convergence, the following equation can be rewritten:

$$\dot{V}_{z1} = \frac{dV_{z1}}{dt} = -\frac{1}{\gamma_z T_{sz} \mu_z} e^{(|V_{1z}|^{\mu_z})} |V_{1z}|^{1-\mu_z} \tag{19}$$

Using some calculations, we obtain

$$\begin{aligned} dt &= -\frac{\gamma_z T_{sz} \mu_z}{e^{(|V_{1z}|^{\mu_z})} |V_{1z}|^{1-\mu_z}} dV_{1z} \\ dt &= -\gamma_z T_{sz} \mu_z e^{-(|V_{1z}|^{\mu_z})} |V_{1z}|^{\mu_z-1} dV_{1z} \end{aligned} \tag{20}$$

By substituting Equation (16), it can be written as $V_{1z} = |e_z| > 0$

$$\int dt = -\gamma_z T_{sz} \mu_z \int V_{1z}^{\mu_z-1} e^{-V_{1z}^{\mu_z}} dV_{z1} \tag{21}$$

Substitute $u = V_{1z}^{\mu_z} \rightarrow du = \mu_z V_{1z}^{\mu_z-1} dV_{1z}$

$$\int dt = -\gamma_z T_{sz} \mu_z \frac{1}{\mu_z} \int e^{-u} du \tag{22}$$

By integrating Equation (22) from t_0 to t_{rz} , one can obtain

$$t_{rz} = t_0 + \gamma_z T_{sz} e^{-u} \tag{23}$$

Undo substitution $u = V_{1z}^{\mu_z}$.

$$t_{rz} = t_0 + \gamma_z T_{sz} e^{-V_{1z}^{\mu_z}} \tag{24}$$

The proof from above is now complete.

The following equation can be obtained from properties (3) and (15),

$$\begin{aligned} \ddot{e}_z(t) &= D^{1+\alpha_z} D^{1-\alpha_z} e_z(t) \\ &= -D^{1+\alpha_z} D^{-\alpha_z} \left\{ \frac{1}{\gamma_z T_{sz} \mu_z} e^{(|e_z|^{\mu_z})} [e_z]^{1-\mu_z} \right\} \\ &= -D^1 \left\{ \frac{1}{\gamma_z T_{sz} \mu_z} e^{(|e_z|^{\mu_z})} [e_z]^{1-\mu_z} \right\} \end{aligned} \tag{25}$$

Therefore, the equivalent controller Π_z can be obtained as follows:

$$\dot{z} - \dot{z}_d = -D^1 \left\{ \frac{1}{\gamma_z T_{sz} \mu_z} e^{(|e_z|^{\mu_z})} [e_z]^{1-\mu_z} \right\} \tag{26}$$

$$\Pi_{zeq} = -D^1 \left\{ \frac{1}{\gamma_z T_{sz} \mu_z} e^{(|e_z|^{\mu_z})} [e_z]^{1-\mu_z} \right\} - \delta_{11} \dot{z} - \mathfrak{d}_z + \dot{z}_d \tag{27}$$

After that, system (7) is designed to reach the PTFO sliding manifolds by the switching controller u_s .

$$\Pi_{zs} = -D^{\alpha_z} \left\{ \frac{1}{T_{cz} \mu_{z2}} e^{(|\sigma_z|^{\mu_{z2}})} [\sigma_z]^{1-\mu_{z2}} + K_z \text{sign}(\sigma_z) \right\} \tag{28}$$

where $T_{cz} > 0$ and μ_{z2}, K_z are positive parameters. Combining (27) and (28), the following law determines the altitude dynamics of the quadrotor:

$$\begin{aligned} \Pi_z = \Pi_{zeq} + \Pi_{zs} &= -D^1 \left\{ \frac{1}{\gamma_z T_{sz} \mu_z} e^{(|e_z|^{\mu_z})} [e_z]^{1-\mu_z} \right\} \\ &\quad - D^{\alpha_z} \left\{ \frac{1}{T_{cz} \mu_{z2}} e^{(|\sigma_z|^{\mu_{z2}})} [\sigma_z]^{1-\mu_{z2}} + K_z \text{sign}(\sigma_z) \right\} - \delta_{11} \dot{z} - \mathfrak{d}_z + \dot{z}_d \end{aligned} \tag{29}$$

Remark 4. The proposed controller is divided into two components. The initial segment incorporates two layers of sliding mode variables and one fractional-order operator. The second component of the proposed controller relies on a fractional-order switching controller. Due to the integration of fractional-order operators in its design, the suggested controller exhibits increased robustness to variations in disturbance frequencies.

4.2. Altitude Stability Analysis for a Quadrotor

Theorem 2. During a predefined time T_{sz} , the proposed control (29) can regulate the consensus error e_{1z} to reach the FOSS.

Proof. Generate the Lyapunov function and the first-order time derivative as follows:

$$\begin{cases} V_{2z} = |\sigma_z| \\ \dot{V}_{2z} = \text{sign}(\sigma_z) \dot{\sigma}_z = \text{sign}(\sigma_z) D^{-\alpha} D^{1+\alpha} \sigma_z \end{cases} \tag{30}$$

$$\dot{V}_{2z} = \text{sign}(\sigma_z) D^{-\alpha} \left(\ddot{e}_z(t) + D^1 \left\{ \frac{1}{T_{sz} \mu_z} e^{(|e_z|^{\mu_z})} [e_z]^{1-\mu_z} \right\} \right) \tag{31}$$

Based on (7) and the PTFOSMC (29), (32) can be yielded as follows:

$$\begin{aligned} \dot{V}_{2z} &= \text{sign}(\sigma_z) \dot{\sigma}_z = \text{sign}(\sigma_z) D^{-\alpha} D^{1+\alpha} \sigma_i \\ &= \text{sign}(\sigma_z) D^{-\alpha} [\delta_{11} \dot{z} + \Pi_z + \mathfrak{d}_z - \dot{z}_d + D^1 \left\{ \frac{1}{T_{sz} \mu_z} e^{(|e_z|^{\mu_z})} [e_z]^{1-\mu_z} \right\}] \end{aligned} \tag{32}$$

$$\begin{aligned} \dot{V}_{2z} = & \text{sign}(\sigma_z) D^{-\alpha} [\delta_{11} \dot{z} - D^1 \{ \frac{1}{T_{sz} \mu_z} e^{(|e_z|^{\mu_z})} [e_z]^{1-\mu_z} \} \\ & - D^{\alpha_z} \{ \frac{1}{T_{cz} \mu_{z2}} e^{(|\sigma_z|^{\mu_{z2}})} |\sigma_z|^{1-\mu_{z2}} + K_z \text{sign}(\sigma_z) \} - \delta_{11} \dot{z} \\ & - \mathfrak{d}_z + \ddot{z}_d + \mathfrak{d}_z - \ddot{z}_d + D^1 \{ \frac{1}{T_{sz} \mu_z} e^{(|e_z|^{\mu_z})} [e_z]^{1-\mu_z} \}] \end{aligned} \tag{33}$$

$$\begin{aligned} \dot{V}_{2z} = & \text{sign}(\sigma_z) D^{-\alpha} [-D^{\alpha_z} \{ \frac{1}{T_{cz} \mu_{z2}} e^{(|\sigma_z|^{\mu_{z2}})} |\sigma_z|^{1-\mu_{z2}} + K_z \text{sign}(\sigma_z) \}] \\ = & - \text{sign}(\sigma_z) [\{ \frac{1}{T_{cz} \mu_{z2}} e^{(|\sigma_z|^{\mu_{z2}})} |\sigma_z|^{1-\mu_{z2}} + K_z \text{sign}(\sigma_z) \}] \end{aligned} \tag{34}$$

Because of $\text{sign}(\sigma) * \text{sign}(\sigma) = 1$, (35) can be achieved as follows:

$$\begin{aligned} \dot{V}_{2z} = & - \text{sign}(\sigma_z) [\{ \frac{1}{T_{cz} \mu_{z2}} e^{(|\sigma_z|^{\mu_{z2}})} |\sigma_z|^{1-\mu_{z2}} \text{sign}(\sigma_z) + K_z \text{sign}(\sigma_z) \}] \\ = & - \frac{1}{T_{cz} \mu_{z2}} e^{(|\sigma_z|^{\mu_{z2}})} |\sigma_z|^{1-\mu_{z2}} |\sigma_z| - K_z |\sigma_z| \end{aligned} \tag{35}$$

$$\dot{V}_{2z} = - \frac{1}{T_{cz} \mu_{z2}} e^{(|V_{2z}|^{\mu_{z2}})} |V_{2z}|^{1-\mu_{z2}} |\sigma_z| - K_z |V_{2z}| \leq 0 \tag{36}$$

□

It can be demonstrated using Theorems 1 and 2 that the consensus error e_z will reach a stable zone in less time than the upper bound time $t \leq T = T_{sz} + T_{cz}$.

As a result, the suggested PTFOSMC can stabilize the quadrotor system to the stable area in the upper bound of the given predefined time T_c .

Remark 5. The position subsystem has three outputs, $(z(t), x(t), y(t))$, but is controlled by only one single control. Hence, the proposed control scheme does not apply to every subsystem. Therefore, to regulate the horizontal position, backstepping with SMC is used.

4.3. Horizontal and Vertical Control Design

In this subsection, the virtual control signals, Π_x and Π_y , will be created by backstepping in conjunction with SMC to provide the desired angles and thrust. The suggested control strategy for the altitude subsystem can ensure that it quickly converges to the required altitude within the predefined time. The sliding mode surfaces for the x and y subsystems can be defined as:

$$\begin{cases} \sigma_x(t) = \dot{e}_x(t) + \lambda_x e_x(t) \\ \sigma_y(t) = \dot{e}_y(t) + \lambda_y e_y(t) \end{cases} \tag{37}$$

Therefore, the time-derivative of these surfaces is as follows:

$$\begin{cases} \dot{\sigma}_x(t) = \ddot{x} - \ddot{x}_d + \lambda_x \dot{e}_x(t) \\ \dot{\sigma}_y(t) = \ddot{y} - \ddot{y}_d + \lambda_y \dot{e}_y(t) \end{cases} \tag{38}$$

Using the controllers created in [33,35], the following laws can be applied to control the horizontal position:

$$\begin{aligned} \Pi_x = & - \delta_9 \dot{x} + \mathfrak{d}_x + \ddot{x}_d(t) - \dot{e}_x(t) \\ & - \lambda_x e_x(t) - K_x \text{sign}(\sigma_x(t)) \\ \Pi_y = & - \delta_{10} \dot{y} + \mathfrak{d}_y + \ddot{y}_d(t) - \dot{e}_y(t) \\ & - \lambda_y e_y(t) - K_y \text{sign}(\sigma_y(t)) \end{aligned} \tag{39}$$

where $\lambda_x, \lambda_y, K_x, K_y > 0$. The predefined-time FOSMC for the attitude subsystem can be designed using the same procedures as those described for altitude in the following subsection.

4.4. Inner-Loop Control Design

The primary issue investigated in this paragraph is how to provide the rolling, pitching, and yawing control inputs in such a way that the rotating subsystem is predefined-time stable.

The following formulas provide the tracking errors for the $\phi(t), \theta(t)$, and $\psi(t)$ subsystems and the time-derivative can be expressed as follows:

$$\begin{cases} e_\phi(t) = \phi(t) + \phi_d(t) \\ e_\theta(t) = \theta(t) + \theta_d(t) \\ e_\psi(t) = \psi(t) + \psi_d(t) \end{cases}, \quad \begin{cases} \dot{e}_\phi(t) = \dot{\phi}(t) + \dot{\phi}_d(t) \\ \dot{e}_\theta(t) = \dot{\theta}(t) + \dot{\theta}_d(t) \\ \dot{e}_\psi(t) = \dot{\psi}(t) + \dot{\psi}_d(t) \end{cases} \quad (40)$$

For subsystems $\phi(t), \theta(t)$, and $\psi(t)$, the predefined-time fractional-order sliding mode manifold is given as

$$\begin{cases} \sigma_\phi = I^{\alpha_\phi} \left\{ \frac{1}{T_{s\phi\mu_\phi}} e^{(|e_\phi|^{\mu_\phi})} [e_\phi]^{1-\mu_\phi} \right\} + \gamma_\phi D^{1-\alpha_\phi} e_\phi(t) \\ \sigma_\theta = I^{\alpha_\theta} \left\{ \frac{1}{T_{s\theta\mu_\theta}} e^{(|e_\theta|^{\mu_\theta})} [e_\theta]^{1-\mu_\theta} \right\} + \gamma_\theta D^{1-\alpha_\theta} e_\theta(t) \\ \sigma_\psi = I^{\alpha_\psi} \left\{ \frac{1}{T_{s\psi\mu_\psi}} e^{(|e_\psi|^{\mu_\psi})} [e_\psi]^{1-\mu_\psi} \right\} + \gamma_\psi D^{1-\alpha_\psi} e_\psi(t) \end{cases} \quad (41)$$

where e_Θ is the error tracking with $\Theta = [\phi, \theta, \psi]$; $T_{s\Theta}$ denotes the predefined setting upper bound convergence time, and $[e_\Theta(t)]^{\mu_{\Theta 2}} = |e_\Theta| \cdot \text{sign}(e_\Theta(t))$ with $0 < \mu_{\Theta 2} < 1$. The following equations can be reached when the consensus error e_Θ reaches the fractional-order sliding surface $\sigma_\Theta = 0$. Considering the use of (41), (42) can be written as follows:

$$\begin{cases} D^{1-\alpha_\phi} e_\phi(t) = -D^{-\alpha_\phi} \left\{ \frac{1}{T_{s\phi\mu_\phi}} e^{(|e_\phi|^{\mu_\phi})} [e_\phi]^{1-\mu_\phi} \right\} \\ D^{1-\alpha_\theta} e_\theta(t) = -D^{-\alpha_\theta} \left\{ \frac{1}{T_{s\theta\mu_\theta}} e^{(|e_\theta|^{\mu_\theta})} [e_\theta]^{1-\mu_\theta} \right\} \\ D^{1-\alpha_\psi} e_\psi(t) = -D^{-\alpha_\psi} \left\{ \frac{1}{T_{s\psi\mu_\psi}} e^{(|e_\psi|^{\mu_\psi})} [e_\psi]^{1-\mu_\psi} \right\} \end{cases} \quad (42)$$

The following equation can be obtained. The following equation can be obtained from properties (3) and (41):

$$\begin{aligned} \ddot{e}_\Theta(t) &= D^{1+\alpha_\Theta} D^{1-\alpha_\Theta} e_\Theta(t) \\ &= -D^{1+\alpha_\Theta} D^{-\alpha_\Theta} \left\{ \frac{1}{T_{s\Theta\mu_\Theta}} e^{(|e_\Theta|^{\mu_\Theta})} [e_\Theta]^{1-\mu_\Theta} \right\} \\ &= -D^1 \left\{ \frac{1}{T_{s\Theta\mu_\Theta}} e^{(|e_\Theta|^{\mu_\Theta})} [e_\Theta]^{1-\mu_\Theta} \right\} \end{aligned} \quad (43)$$

Therefore, the equivalent controller Π_j with $j = 2, 3, 4$ can be obtained as follows:

$$\ddot{\Theta} - \ddot{\Theta}_d = -D^1 \left\{ \frac{1}{T_{s\Theta\mu_\Theta}} e^{(|e_\Theta|^{\mu_\Theta})} [e_\Theta]^{1-\mu_\Theta} \right\} \quad (44)$$

$$\Pi_{jeq} = -D^1 \left\{ \frac{1}{T_{s\Theta\mu_\Theta}} e^{(|e_\Theta|^{\mu_\Theta})} [e_\Theta]^{1-\mu_\Theta} \right\} - f(\Theta) \quad (45)$$

By substituting Equation (45) into Equation (7), the equivalent controller of attitude can be written as

$$\begin{cases} \Pi_{2eq} = -J_x D^1 \left\{ \frac{1}{T_{s\phi\mu\phi}} e^{(|e_\phi|^{\mu_\phi})} [e_\phi]^{1-\mu_\phi} \right\} - \delta_1 \dot{\theta} \dot{\psi} - \delta_2 \omega_r \dot{\theta}^2 - \delta_3 \dot{\phi} - \mathfrak{d}_\phi \\ \Pi_{3eq} = -J_y D^1 \left\{ \frac{1}{T_{s\phi\mu\phi}} e^{(|e_\phi|^{\mu_\phi})} [e_\phi]^{1-\mu_\phi} \right\} - \delta_4 \dot{\phi} \dot{\psi} - \delta_5 \omega_r \dot{\phi}^2 - \delta_6 \dot{\theta} - \mathfrak{d}_\theta \\ \Pi_{4eq} = -J_z D^1 \left\{ \frac{1}{T_{s\psi\mu\psi}} e^{(|e_\psi|^{\mu_\psi})} [e_\psi]^{1-\mu_\psi} \right\} - \delta_7 \dot{\phi} \dot{\theta} - \delta_8 \dot{\psi} - \mathfrak{d}_\psi \end{cases} \quad (46)$$

System (7) is then constructed to use the switching controller, u_s , to reach the PTFO sliding manifolds.

$$\Pi_{\Theta s} = -D^{\alpha_\Theta} \left\{ \frac{1}{T_{c\Theta\mu_{\Theta 2}}} e^{(|\sigma_\Theta|^{\mu_{\Theta 2}})} [\sigma_\Theta]^{1-\mu_{\Theta 2}} \right. \quad (47)$$

$$\left. + K_\Theta \text{sign}(\sigma_\Theta) \right\} \quad (48)$$

where $T_{c\Theta} > 0$ and $\mu_{\Theta 2}, K_\Theta$ are positive parameters with $\Theta = [\phi, \theta, \psi]$. Combining (46) and (48), the following law determines the altitude dynamics of the quadrotor:

$$\begin{aligned} \Pi_\Theta &= \Pi_{\Theta eq} + \Pi_{\Theta s} \\ &= -D^1 \left\{ \frac{1}{T_{s\Theta\mu_\Theta}} e^{(|e_\Theta|^{\mu_\Theta})} [e_\Theta]^{1-\mu_\Theta} \right\} - f(\Theta) \\ &\quad - D^{\alpha_\Theta} \left\{ \frac{1}{T_{c\Theta\mu_{\Theta 2}}} e^{(|\sigma_\Theta|^{\mu_{\Theta 2}})} [\sigma_\Theta]^{1-\mu_{\Theta 2}} + K_\Theta \text{sign}(\sigma_\Theta) \right\} \end{aligned} \quad (49)$$

The corresponding PTFOSM controller for the quadrotor attitude is given as

$$\begin{aligned} \Pi_2 &= -J_x D^1 \left\{ \frac{1}{T_{s\phi\mu_\phi}} e^{(|e_\phi|^{\mu_\phi})} [e_\phi]^{1-\mu_\phi} \right\} - \delta_1 \dot{\theta} \dot{\psi} - \delta_2 \omega_r \dot{\theta}^2 - \delta_3 \dot{\phi} \\ &\quad + K_\phi \text{sign}(\sigma_\phi) \left\} - \mathfrak{d}_\phi + \ddot{\phi}_d - D^{\alpha_\phi} \left\{ \frac{1}{T_{c\phi\mu_{\phi 2}}} e^{(|\sigma_\phi|^{\mu_{\phi 2}})} [\sigma_\phi]^{1-\mu_{\phi 2}} \right. \end{aligned} \quad (50)$$

$$\begin{aligned} \Pi_3 &= -J_y D^1 \left\{ \frac{1}{T_{s\phi\mu_\phi}} e^{(|e_\phi|^{\mu_\phi})} [e_\phi]^{1-\mu_\phi} \right\} - \delta_4 \dot{\phi} \dot{\psi} - \delta_5 \omega_r \dot{\phi}^2 - \delta_6 \dot{\theta} - \mathfrak{d}_\theta \\ &\quad + K_\theta \text{sign}(\sigma_\theta) \left\} - \mathfrak{d}_\theta + \ddot{\phi}_d - D^{\alpha_\theta} \left\{ \frac{1}{T_{c\theta\mu_{\theta 2}}} e^{(|\sigma_\theta|^{\mu_{\theta 2}})} [\sigma_\theta]^{1-\mu_{\theta 2}} \right. \end{aligned} \quad (51)$$

$$\begin{aligned} \Pi_4 &= -J_z D^1 \left\{ \frac{1}{T_{s\psi\mu_\psi}} e^{(|e_\psi|^{\mu_\psi})} [e_\psi]^{1-\mu_\psi} \right\} - \delta_7 \dot{\phi} \dot{\theta} - \delta_8 \dot{\psi} \\ &\quad + K_\psi \text{sign}(\sigma_\psi) \left\} - \mathfrak{d}_\psi + \ddot{\phi}_d - D^{\alpha_\psi} \left\{ \frac{1}{T_{c\psi\mu_{\psi 2}}} e^{(|\sigma_\psi|^{\mu_{\psi 2}})} [\sigma_\psi]^{1-\mu_{\psi 2}} \right. \end{aligned} \quad (52)$$

Remark 6. The reaching law proposed in this paper has two main advantages: (1) it guarantees the predefined time convergence of the sliding manifold and (2) it copes with complex disturbances.

4.5. Attitude Stability Analysis for a Quadrotor

Theorem 3. The errors will achieve convergence to the origin within a predefined time for the fractional-order sliding surface, and stability for the yaw subsystem is attained as the state errors are fulfilled.

Proof. The selection of the Lyapunov function for the quadrotor system is as follows:

$$V_{1\psi} = |e_\psi| \quad (53)$$

The time differentiation of V_{1i} is achieved as follows:

$$\begin{aligned}
 \dot{V}_{1\psi} &= \text{sign}(e_\psi) \dot{e}_\psi = \text{sign}(e_\psi) D^\alpha D^{1-\alpha} e_\psi \\
 &= \text{sign}(e_\psi) D^\alpha \left(-D^{-\alpha\psi} \frac{1}{T_{s\psi} \mu_\psi} e^{(|e_\psi|^{\mu_\psi})} [e_\psi]^{1-\mu_\psi} \right) \\
 &= \text{sign}(e_\psi) \left(-\frac{1}{T_{s\psi} \mu_\psi} e^{(|e_\psi|^{\mu_\psi})} [e_\psi]^{1-\mu_\psi} \right)
 \end{aligned} \tag{54}$$

Due to $\text{sign}(e_\psi) \times \text{sign}(e_\psi) = 1$, (18) can be achieved as follows:

$$\begin{aligned}
 \dot{V}_{\psi 1} &= \text{sign}(e_\psi) \left(-\frac{1}{T_{s\psi} \mu_\psi} e^{(|e_\psi|^{\mu_\psi})} \text{sign}(e_i) |e_\psi|^{1-\mu_\psi} \right) \\
 &= -\frac{1}{T_{s\psi} \mu_\psi} e^{(|e_\psi|^{\mu_\psi})} |e_\psi|^{1-\mu_\psi} \\
 &= -\frac{1}{T_{s\psi} \mu_\psi} e^{(|V_{1\psi}|^{\mu_\psi})} |V_{1\psi}|^{1-\mu_\psi} \leq 0
 \end{aligned} \tag{55}$$

□

Based on Lemma 2, it is demonstrated that the dynamic system (system (55)) can converge to zero in a predefined time $T_{s\psi}$.

The fractional-order sliding surface σ_ψ will converge to zero if the dynamic system in (42) is stable.

Theorem 4. Consider the PTFO sliding manifold designed in (42); the convergence to zero in a predefined time of the dynamics system defined in (7) is ensured.

Proof. To prove Theorem 4, the Lyapunov function candidate of the yaw- subsystem is considered as follows:

$$\begin{cases} V_3 = |\sigma_\psi| \\ \dot{V}_3 = \text{sign}(\sigma_\psi) \dot{\sigma}_\psi = \text{sign}(\sigma_\psi) D^{-\alpha} D^{1+\alpha} \sigma_\psi \end{cases} \tag{56}$$

$$\dot{V}_{2\psi} = \text{sign}(\sigma_\psi) D^{-\alpha} \left(\ddot{e}_\psi(t) + D^1 \left\{ \frac{1}{T_{s\psi} \mu_\psi} e^{(|e_\psi|^{\mu_\psi})} [e_\psi]^{1-\mu_\psi} \right\} \right) \tag{57}$$

Based on (7) and the PTFOSMC (49), (32) can be yielded as follows:

$$\begin{aligned}
 \dot{V}_{2\psi} &= \text{sign}(\sigma_\psi) \dot{\sigma}_\psi = \text{sign}(\sigma_\psi) D^{-\alpha} D^{1+\alpha} \sigma_i \\
 &= \text{sign}(\sigma_\psi) D^{-\alpha} [\delta_7 \dot{\phi} \dot{\theta} + \delta_8 \dot{\psi} + \mathfrak{d}_\psi + J_z^{-1} \Pi_4 \\
 &\quad - \ddot{\psi}_d + D^1 \left\{ \frac{1}{T_{s\psi} \mu_\psi} e^{(|e_\psi|^{\mu_\psi})} [e_\psi]^{1-\mu_\psi} \right\}]
 \end{aligned} \tag{58}$$

$$\begin{aligned}
 \dot{V}_{2\psi} &= \text{sign}(\sigma_\psi) D^{-\alpha} [\delta_7 \dot{\phi} \dot{\theta} + \delta_8 \dot{\psi} + \mathfrak{d}_\psi - \ddot{\psi}_d - \delta_7 \dot{\phi} \dot{\theta} - \delta_8 \dot{\psi} - \mathfrak{d}_\psi + \ddot{\psi}_d \\
 &\quad + J_z^{-1} [-J_z D^1 \left\{ \frac{1}{T_{s\psi} \mu_\psi} e^{(|e_\psi|^{\mu_\psi})} [e_\psi]^{1-\mu_\psi} \right\} - K_\psi \text{sign}(\sigma_\psi) \}} \\
 &\quad - D^{\alpha\psi} \left\{ \frac{1}{T_{c\psi} \mu_{\psi 2}} e^{(|\sigma_\psi|^{\mu_{\psi 2}})} [\sigma_\psi]^{1-\mu_{\psi 2}} + D^1 \left\{ \frac{1}{T_{s\psi} \mu_\psi} e^{(|e_\psi|^{\mu_\psi})} [e_\psi]^{1-\mu_\psi} \right\} \right\} \\
 &= -\text{sign}(\sigma_\psi) D^{-\alpha\psi} [K_\psi \text{sign}(\sigma_\psi) + D^{\alpha\psi} \left\{ \frac{1}{T_{c\psi} \mu_{\psi 2}} e^{(|\sigma_\psi|^{\mu_{\psi 2}})} [\sigma_\psi]^{1-\mu_{\psi 2}} \right\}] \\
 &= -K_\psi |\sigma_\psi| - D^{\alpha\psi} \left\{ \frac{1}{T_{c\psi} \mu_{\psi 2}} e^{(|\sigma_\psi|^{\mu_{\psi 2}})} |\sigma_\psi|^{1-\mu_{\psi 2}} |\sigma_\psi| \right\}
 \end{aligned} \tag{59}$$

$$\dot{V}_{2\psi} = -K_\psi |V_3| - D^{\alpha\psi} \left\{ \frac{1}{T_{c\psi} \mu_{\psi 2}} e^{(|V_3|^{\mu_{\psi 2}})} |V_3|^{1-\mu_{\psi 2}} |V_3| \right\} \leq 0. \tag{60}$$

□

It can be demonstrated using Theorems 3 and 4 that the consensus error e_ψ will reach a stable zone in less time than the upper bound time $t \leq T_2 = T_{s\psi} + T_{c\psi}$.

It is clear from the analysis above that the reaching condition of attitude loop stability is ensured.

Example 1. The suggested controller is used to stabilize the yaw subsystem using the settings listed in Tables 1 and 2. The examples in Figures 3 and 4 represent the simulation results for this example. The sliding manifold and the state variable of the yaw subsystem both converge to their origins within the predefined time T_f , as can be seen from these results. As illustrated in Figure 3, the smaller the parameters, T_c and T_s , the less serious the control, indicating that choosing the appropriate T_c and T_s is important in practical implementations of the recommended control approach, as in Figure 3.

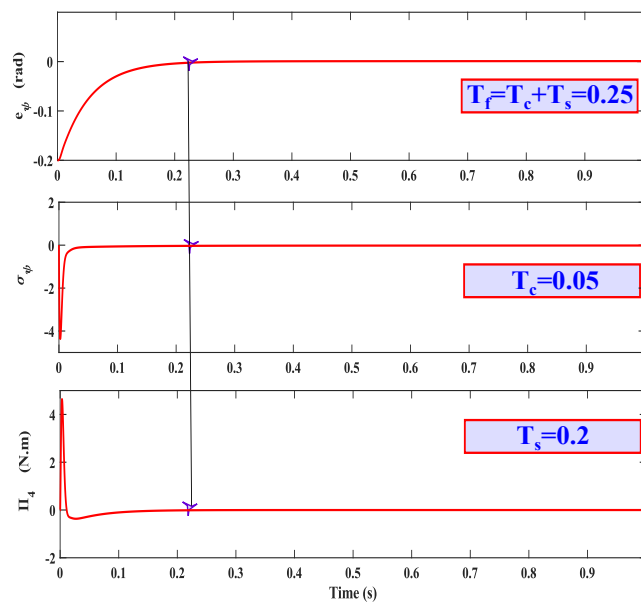


Figure 3. Result e_ψ , σ_ψ , and Π_4 with $T_c = 0.05$ and $T_s = 0.2$.

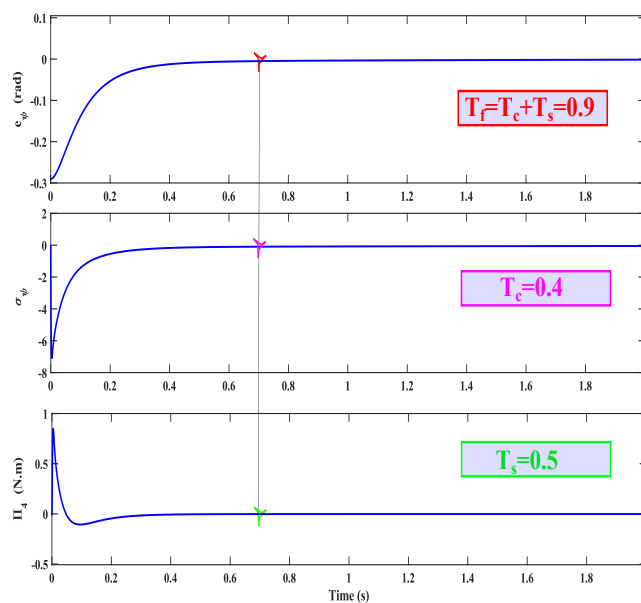


Figure 4. Results e_ψ , σ_ψ , and Π_4 with $T_c = 0.4$ and $T_s = 0.5$.

Table 1. Quadrotor physical characteristics.

Symbol	Value	Symbol	Value
m (kg)	0.74	k_x ($m^{-1} \cdot s \cdot N$)	5.5670×10^{-4}
g ($s^{-2} \cdot m$)	9.81	k_y ($m^{-1} \cdot s \cdot N$)	5.5670×10^{-4}
l (m)	0.5	k_z ($m^{-1} \cdot s \cdot N$)	5.5670×10^{-4}
J_r ($kg \cdot m^2$)	2.03×10^{-5}	K_{ax} ($rad^{-1} \cdot s \cdot N$)	5.5670×10^{-4}
J_x ($kg \cdot m^2$)	0.004	K_{ay} ($rad^{-1} \cdot s \cdot N$)	5.5670×10^{-4}
J_y ($kg \cdot m^2$)	0.004	K_{az} ($rad^{-1} \cdot s \cdot N$)	5.5670×10^{-4}
J_z ($kg \cdot m^2$)	0.0084	b ($s^2 \cdot N$)	2.984×10^{-3}

Table 2. Control parameters.

Parameter	Value	Parameter	Value
$T_{c1,c3,c5}$	0.8	T_{cz}	2
$T_{s\phi,s\theta,s\psi}$	0.5	T_{sz}	1
$k_{\phi,\theta,\psi}$	10.51	k_z	5
$\gamma_{\phi,\theta,\psi}$	20	γ_z	4
$\mu_{\phi,\theta,\psi}$	0.2	μ_z	0.9
$\mu_{\phi2,\theta2,\psi2}$	0.4	μ_{z2}	0.9

4.6. Stability Global Analysis

Theorem 5. Fundamental control law Equations (36) and (59) applied to the investigated system (7) guarantee the overall quadrotor system stability.

Proof. The Lyapunov function for the quadrotor system and its time-derivative are given as follows:

$$\begin{cases} V_g = V_{2z} + V_{2\phi} + V_{2\theta} + V_{2\psi} \\ \dot{V}_g = \dot{V}_{2z} + \dot{V}_{2\phi} + \dot{V}_{2\theta} + \dot{V}_{2\psi} \end{cases} \tag{61}$$

From Equations (36) and (60), we have

$$\begin{aligned} V_g &= -\frac{1}{T_{cz}\mu_{z2}} e^{(|\sigma_z|^{\mu_{z2}})} |\sigma_z|^{1-\mu_{z2}} |\sigma_z| - K_z |\sigma_z| \\ &\quad - D^{\alpha_\phi} \left\{ \frac{1}{T_{c\phi}\mu_{\phi2}} e^{(|\sigma_\phi|^{\mu_{\phi2}})} |\sigma_\phi|^{1-\mu_{\phi2}} |\sigma_\phi| \right\} \\ &\quad - D^{\alpha_\theta} \left\{ \frac{1}{T_{c\theta}\mu_{\theta2}} e^{(|\sigma_\theta|^{\mu_{\theta2}})} |\sigma_\theta|^{1-\mu_{\theta2}} |\sigma_\theta| \right\} \\ &\quad - D^{\alpha_\psi} \left\{ \frac{1}{T_{c\psi}\mu_{\psi2}} e^{(|\sigma_\psi|^{\mu_{\psi2}})} |\sigma_\psi|^{1-\mu_{\psi2}} |\sigma_\psi| \right\} \\ &\quad - K_\phi |\sigma_\phi| - K_\theta |\sigma_\theta| - K_\psi |\sigma_\psi| \leq 0. \end{aligned} \tag{62}$$

According to Theorems 1–4, Theorem 5 demonstrates the global stability achieved for both rotational and translational tracking errors through the Lyapunov approach. □

Remark 7. The quadrotor system control has two loops, where the inner loop (attitude loop) is faster compared to the outer loop (position loop). The proposed PTFOSMC has been successfully applied to the inner loop to achieve predefined time performances and the z-subsystem has benefited from the proposed controller.

Remark 8. The proposed scheme offers several advantages, including the predefined-time convergence of system states, predefined-time convergence in the sliding mode phase, mitigation of the chattering problem, resilience to bounded external disturbances, and heightened robustness.

5. Simulations Results for Quadrotor

In this section, numerical simulations are used to assess the effectiveness of the suggested control approach, which is based on the PTFOSMC method for the path-following problem. The physical characteristics of a quadrotor are listed in Table 1. In Table 2, the PTFOSMC parameters are displayed.

Remark 9. The resolution to the chattering problem involves transforming the discontinuous element function into a continuous function, such as the hyperbolic tangent function.

5.1. Scenario 1

In this case, the quadrotor tracks the desired reference without external disturbances. Equation (63) provides more particular information about the desired trajectory.

$$\begin{cases} x_d = 0.5 \cos(\frac{\pi}{20})m, & y_d = 0.5 \sin(\frac{\pi}{20})m & z_d = 2 - 2 \cos(\frac{\pi}{2})m \\ \psi_d = 0.4 \text{ rad } t \in [0 \ 50] \text{ and } \psi_d = 0.2 \text{ rad } t \in [50 \ 80] \end{cases} \quad (63)$$

The tracking abilities of the PTFOSMC without disturbances are displayed in Figures 5–7. A good tracking trajectory is produced by the position subsystem’s suggested control strategy, as shown in Figure 5. Moreover, the tracking performance of the yaw, pitch, and roll angles as they converge to their origin values in a predefined time is presented in Figure 6. As seen in this Figure, the yaw, for example, converges to the origin before the predefined time $T_{s\psi} = T_{s\psi1} + T_{s\psi2} = 0.3$ s. In addition, one can see that controller u remains continuous and the sliding mode $\sigma_{\psi} = 0$ is required for every $t \geq T_{s\psi2}$. Figure 7 shows an excellent tracking trajectory of the desired control without external disturbances.

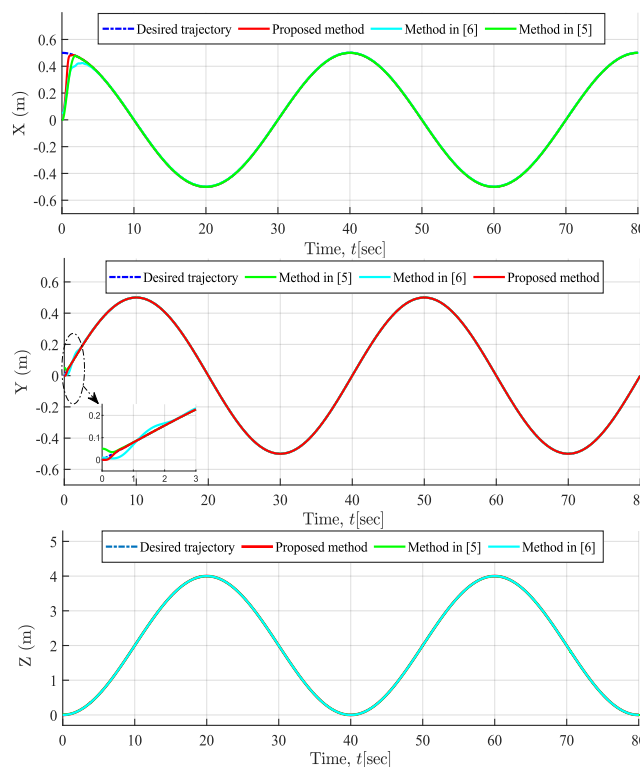


Figure 5. Quadrotor position without disturbances.

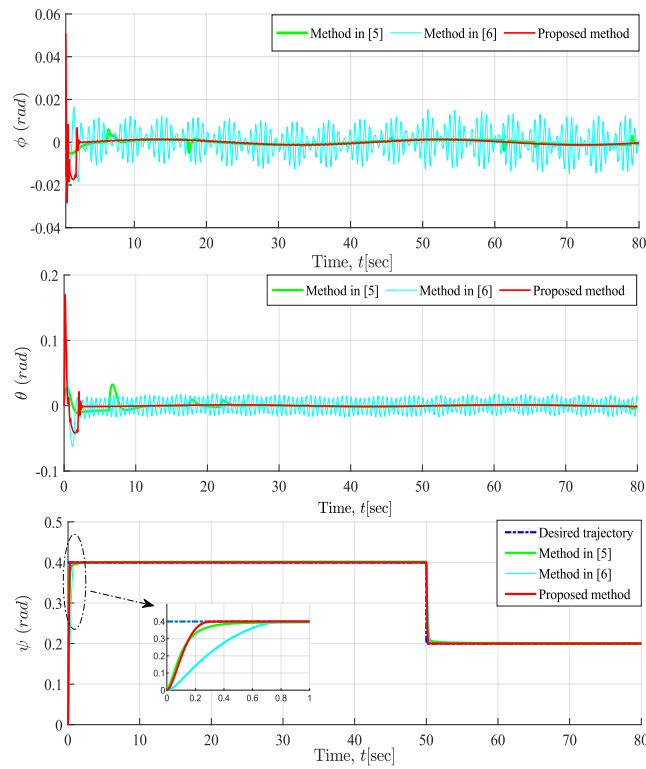


Figure 6. Quadrotor attitude without disturbances.

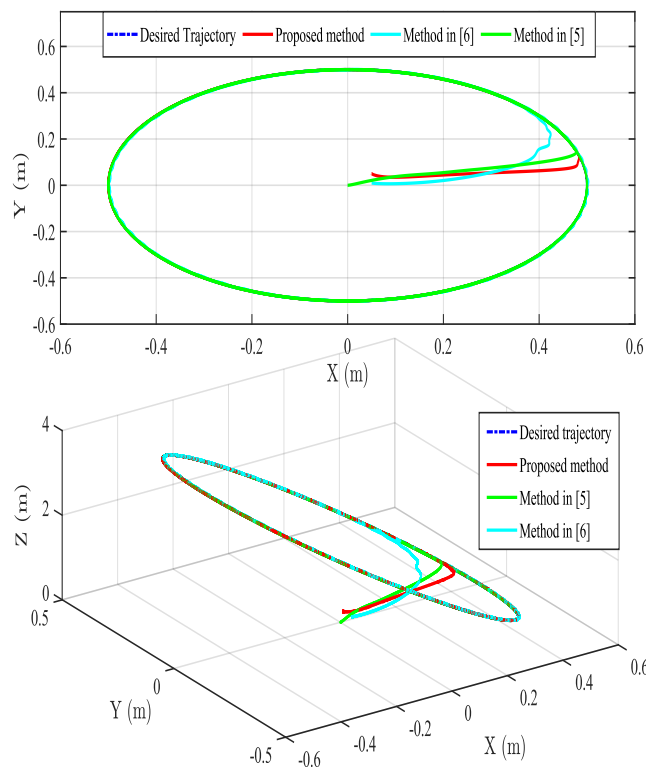


Figure 7. The 2D and 3D trajectories of a quadrotor without disturbances.

5.2. Scenario 2

This section is used to assess the stability of a quadrotor when it encounters time-varying disturbances. Quadrotor model equations are expanded to include disturbances. One assumes that the disturbances should be bounded. When the quadrotor flies outside,

wind gusts cause these disruptions, which are accelerations. As a result, disturbances are shown in the following ways:

$$\begin{cases} \partial_x = 0.5 \sin(0.4t) \text{ m/s}^2 & 10 < t < 30 \\ \partial_y = 0.2 \sin(0.4t) + 0.3 \cos(0.7t) \text{ m/s}^2 & 10 < t < 50 \\ \partial_z = 0.4 \cos(0.7t) \text{ m/s}^2 & t > 20 \\ \partial_\phi = 0.3 \cos(0.4t) \text{ rad/s}^2 & t < 10 \\ \partial_\theta = 0.3 \cos(0.5t) \text{ rad/s}^2 & 10 < t < 20 \\ \partial_\psi = 0.3 \cos(0.7t) \text{ rad/s}^2 & t > 20 \end{cases} \quad (64)$$

Equations (65) and (66) provide the desired trajectory.

$$\begin{cases} x_d = 0.5 \cos(t/2)m & t \in [0, 4\pi] \\ x_d = 0.5m & t \in [4\pi, 20] \\ x_d = 0.25t - 4.5m & t \in [20, 30] \\ x_d = 3m & t \in [30, 80] \end{cases}, \begin{cases} y_d = 0.5 \sin(t/2)m & t \in [0, 4\pi] \\ y_d = 0.25t - 3.14m & t \in [4\pi, 20] \\ y_d = 5 - \pi m & t \in [20, 30] \\ y_d = -0.2358t + 8.94m & t \in [4\pi, 20] \\ y_d = -0.5m & t \in [30, 80] \end{cases} \quad (65)$$

$$\begin{cases} z_d = 0.125t + 1 \text{ m} & t \in [0, 4\pi] \\ z_d = 0.5\pi + 1 \text{ m} & t \in [4\pi, 40] \\ z_d = \exp(-0.2t + 8.944) \text{ m} & t \in [40, 80] \end{cases}, \begin{cases} \psi_d = 0.4rad & t \in [0, 50] \\ \psi_d = 0.2rad & t \in [50, 80] \end{cases} \quad (66)$$

The tracking results obtained in scenario 2 (Figures 8–13) demonstrate the effectiveness of the control strategy suggested in this work. The proposed nonlinear control law was found to perform better than the ABSMC and PIDSMC control laws developed in [9,10] for the control of present external disturbances during the flight and following the desired trajectory. The performance attitude and position in terms of tracking performance are shown in Figures 8 and 9. In this regard, the proposed control system provides a shorter settling time than various other controls and we can see that the position and attitude controllers are accurate in tracking the correct values even when the references change quickly. We present the effectiveness of the control inputs of the quadrotor ($\Pi_1, \Pi_2, \Pi_3, \Pi_4$). As can be seen, the smooth convergence of the control signals to their original values (7.2598, 0, 0, 0) illustrates the efficiency of the PTFOSMC technique. The tracking sliding manifolds made by the system are shown in Figures 11 and 12. These data demonstrate that the tracking surfaces maintain their status of zero. The 3D flight trajectory is depicted in Figure 13. The results presented above show that, in comparison to previous techniques, the PTFOSMC has successfully tracked the desired trajectory.

5.3. Scenario 3

To further evaluate the effectiveness of the PTFOSMC method, the disturbances mentioned in scenario 2 are added to all state variables. In the current case, the initial conditions are changed; for the yaw subsystem, $\psi_0 = 0.2 \text{ rad}$, $\psi_0 = 0.4 \text{ rad}$, and $\psi_0 = 0.8 \text{ rad}$, for the z-subsystem, $z_0 = 0 \text{ m}$, $z_0 = 0.2 \text{ m}$, $z_0 = 0.5 \text{ m}$, and $z_0 = 0.8 \text{ m}$.

The response of the quadrotor system provides evidence that the suggested controller induces a fast response. It should also be noted that there is an upper constraint on the convergence time, which can be predefined as an adjustable control parameter and is independent of the initial conditions, as shown in Figure 14.

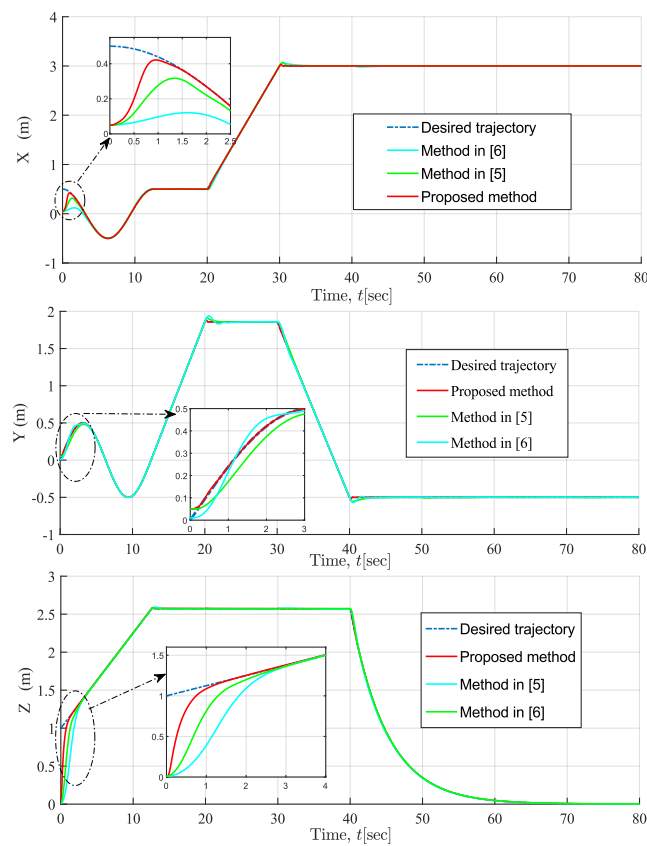


Figure 8. Position of a quadrotor.

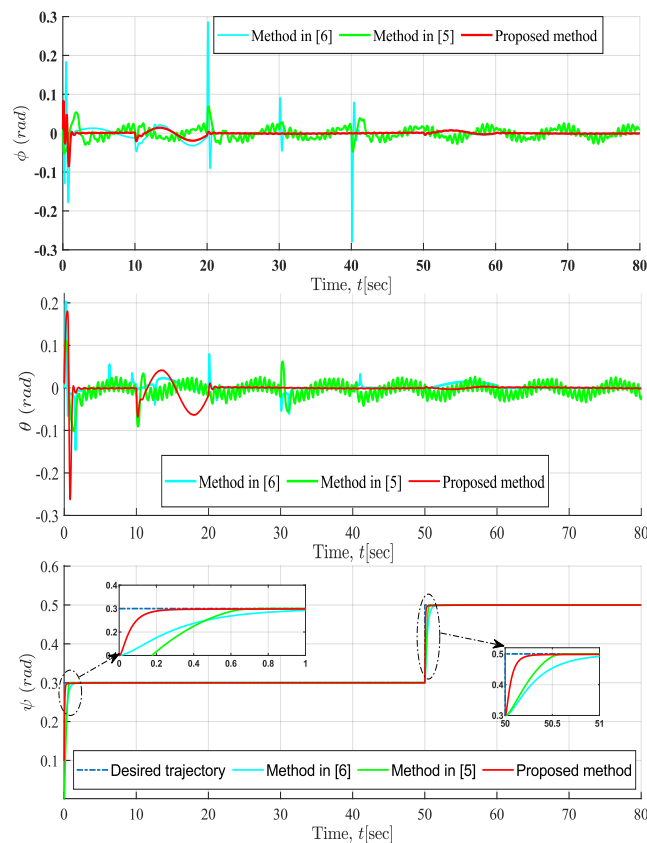


Figure 9. Attitude of a quadrotor.

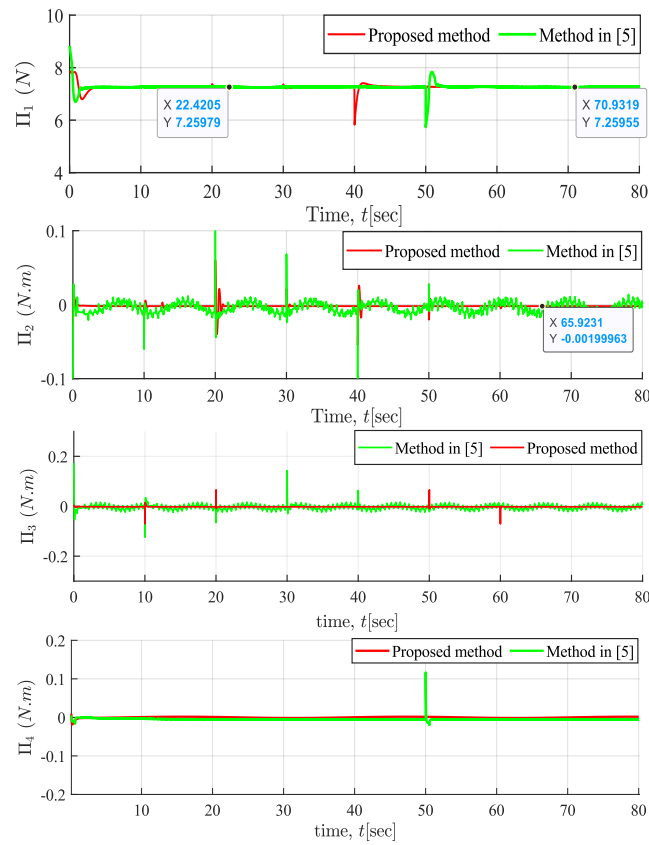


Figure 10. Inputs a quadrotor.

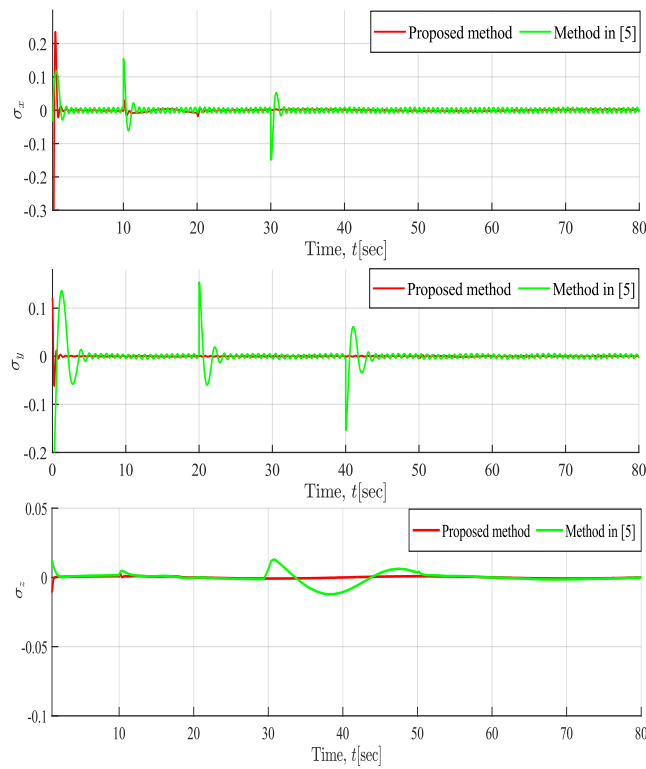


Figure 11. Sliding surface for the position subsystem.

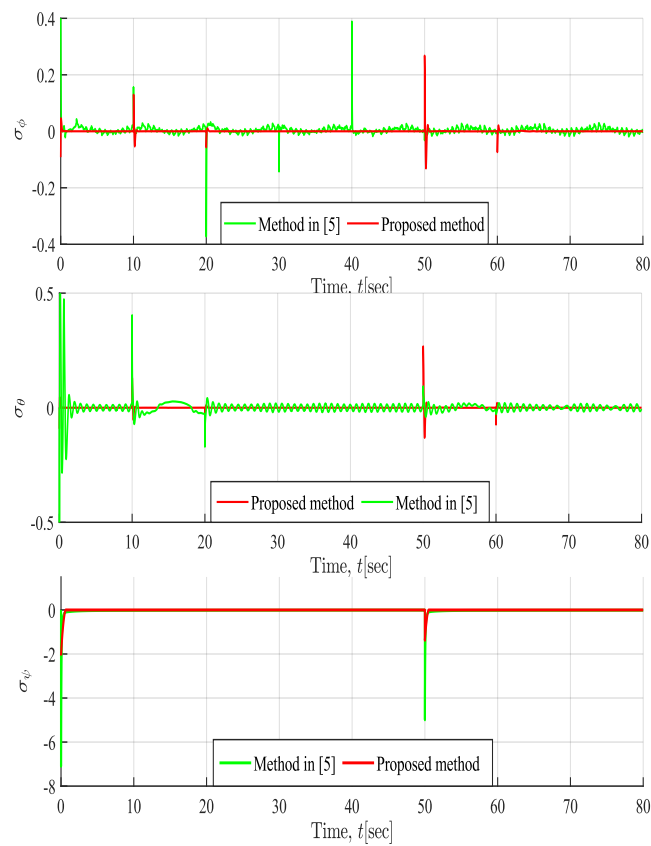


Figure 12. Sliding surface for the attitude subsystem.

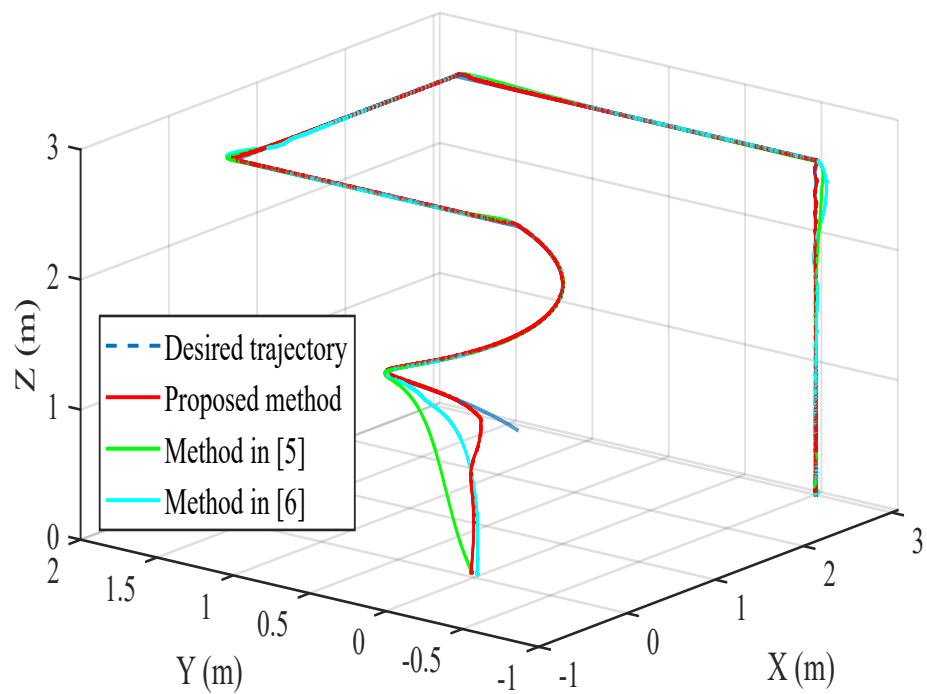


Figure 13. The 3D trajectories of a quadrotor.

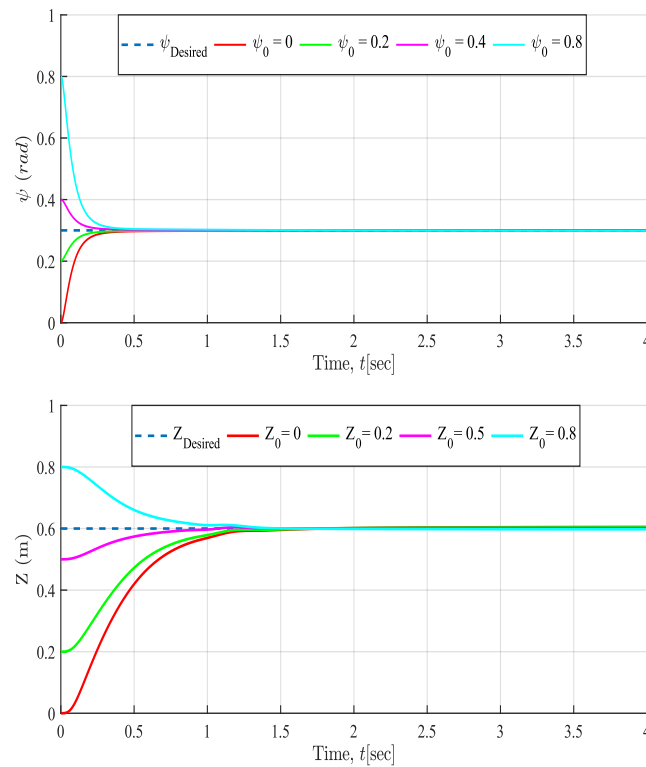


Figure 14. Initial values of a quadrotor.

5.4. Quantitative Analysis of the Controllers

The preceding curves are used to demonstrate the differences between the controllers because all the strategies produce acceptable results in the ideal scenario. As a result, the performance indices, ISE and ISV, are provided as objective functions to be utilized in the next part.

- Integral square error (ISE): It is given by $ISE = \int_{t_0}^{e_t} (e^2(t)) dt$
- Integral of the square value of control signal (ISV): $ISV = \int_{t_0}^{t_t} \Pi^2(t) dt$

Table 3 shows the ISE performance of the three controllers. The proposed method is superior to previous techniques since it can be established through the PTFOSM control that the ISE indices are lower than BSMC and PIDSMC. Moreover, we also notice that the proposed control uses less energy than PIDSMC and the other way around.

Table 3. Performance index of ISE.

ISE of the Scenario 1			
Variable	Proposed Method	Method [5]	Method [6]
$\phi(t)$	0.001698	0.003314	0.03161
$\theta(t)$	0.004448	0.0105	0.03038
$\psi(t)$	0.009245	0.2262	0.01622
$z(t)$	0.2036	0.3646	0.4262
ISE of the Scenario 2			
Variable	Proposed Method	Method [5]	Method [6]
$\phi(t)$	0.000202	0.000948	0.001744
$\theta(t)$	0.006334	0.003576	0.007545
$\psi(t)$	0.009247	0.022640	0.016220
$z(t)$	4.26×10^{-6}	3.76×10^{-6}	0.000410

The three controllers demonstrate satisfactory performance with moderate energy consumption, regardless of external influences. However, the presence of an additional

payload, such as a gust of wind, necessitates extra thrust to ensure optimal performance. As evident from Table 3 and in the second scenario, the PIDSMC technique exhibits the least accuracy ($ISE_\psi = 0.01622$), followed by the classical MFC technique, ($ISE_\psi = 0.02264$), whereas PTFOSMC proves to be the most accurate ($ISE_\psi = 0.009247$). Additionally, it is observed that PIDSMC consumes more energy, while the proposed control consumes less energy.

Table 4 presents the ISV comparative results for the inputs of a quadrotor. It is clear that the performance index values for the proposed control methodology are significantly lower than those for the alternative strategy. The tracking performance of the suggested control approach is then found to be better than that of the method of [9,10] by comparing the simulation results.

Table 4. Performance index of ISV.

ISV of the Scenario 1			
Variable	Proposed Method	Method [5]	Method [6]
Total thrust	7.259	7.26	7.3
Total torques	0.003153	0.003772	−0.003348
ISV of the Scenario 2			
Variable	Proposed Method	Method [5]	Method [6]
Total thrust	7.259	7.265	7.32
Total torques	0.0002127	0.002856	−0.0002931

Remark 10. *The proposed control approach was compared to the BSMC and PIDSMC techniques in addressing the quadrotor system tracking issue. While tracking errors in other approaches may only converge to a bounded neighborhood of the origin within a predefined time due to the use of an error as a sliding variable, the suggested control scheme, incorporating a fractional-order manifold, ensures the predefined-time zero-error stability of quadrotor systems, leading to enhanced steady-state performance.*

Remark 11. *In this paper, two nonlinear surfaces are introduced to achieve the finite-time convergence of the quadrotor states.*

Remark 12. *The benefits of the suggested fractional-order predefined-time sliding mode controllers include predefined-time convergence of system states, predefined-time convergence in the reaching phase, alleviation of the chattering phenomenon, and the incorporation of an additional fractional-order differential element that remains insensitive to bounded external disturbances.*

The implementation challenges of the proposed control method for the quadrotor’s position and attitude will be examined through four simulations. The complexity of the problem arises from addressing tracking performance, which includes convergence time and steady-state performance for both inner and outer loops, especially in the presence of external disturbances. Moreover, the innovation of the proposed control lies in the formulation of a predefined-time controller based on fractional-order sliding mode control, enhancing the robustness and precision of the quadrotor system.

6. Conclusions

This work suggests a novel control method for tracking quadrotor trajectory. Novel predefined time in fractional-order sliding mode manifolds are developed to stabilize tracking errors to the origin within a predefined time. A systematic evaluation is conducted on the quadrotor system to verify specific conditions on the control parameters, ensuring the stability of zero tracking error. The Newton–Euler method is applied in this research to determine the dynamics of the quadrotor. The SMC can ensure that the quadrotor system will obtain better dynamic performances due to its benefits of quick transient

response, high resilience, and simple implementation. The proposed strategy is employed to govern a quadrotor system across various scenarios influenced by escalating disturbance amplitudes and frequencies. Additionally, the PTFOSMC is designed using fractional calculus to reduce the inherent chattering problem of the standard SMC and improve parameter freedom. The simulation findings demonstrate that the quadrotor system using the proposed PTFOSMC might exceed existing control strategies with faster convergence time and higher robustness.

Author Contributions: Conceptualization, A.B., M.L. and S.B.; Methodology, A.B., M.L., S.B. and F.S.A.; Software, A.B. and M.L.; Validation, M.L., S.B., F.S.A. and M.B.; Formal analysis, A.B., M.L. and F.S.A.; Writing—original draft, A.B. and M.L.; Visualization, M.L., S.B. and M.B.; Supervision, M.L., F.S.A. and M.B.; funding acquisition, S.B. and F.S.A. All authors have read and agreed to the published version of the manuscript.

Funding: Deputyship for Research & Innovation, Ministry of Education in Saudi Arabia—project number MoE-IF-UJ-22-04220772-6.

Data Availability Statement: No data were used to support this study.

Acknowledgments: The authors extend their appreciation to the Deputyship for Research & Innovation, Ministry of Education in Saudi Arabia for funding this research work through project number MoE-IF-UJ-22-04220772-6.

Conflicts of Interest: The authors declare no conflict of interest.

References

- Hassanaliam, M.; Abdelkefi, A. Classifications, Applications, and Design Challenges of Drones: A Review. *Prog. Aerosp. Sci.* **2017**, *91*, 99–131. [[CrossRef](#)]
- Watts, A.C.; Ambrosia, V.G.; Hinkley, E. Unmanned Aircraft Systems in Remote Sensing and Scientific Research: Classification and Considerations of Use. *Remote Sens.* **2012**, *4*, 1671–1692. [[CrossRef](#)]
- de Zarzà, I.; de Curtò, J.; Cano, J.C.; Calafate, C.T. Drone-Based Decentralized Truck Platooning with UWB Sensing and Control. *Mathematics* **2023**, *11*, 4627. [[CrossRef](#)]
- Eskandaripour, H.; Boldsai Khan, E. Last-Mile Drone Delivery: Past, Present, and Future. *Drones* **2023**, *7*, 77. [[CrossRef](#)]
- Gohari, A.; Ahmad, A.; Rahim, R.A.; Supa'at, A.S.M.; Razak, S.A.; Gismalla, M.S.M. Involvement of Surveillance Drones in Smart Cities: A Systematic Review. *IEEE Access* **2022**, *10*, 56611–56628. [[CrossRef](#)]
- Mishra, B.; Garg, D.; Narang, P.; Mishra, V.K. Drone-surveillance for Search and Rescue in Natural Disaster. *Comput. Commun.* **2020**, *156*, 1–10. [[CrossRef](#)]
- Labbadi, M.; Cherkaoui, M. Robust Adaptive Nonsingular Fast Terminal Sliding-mode Tracking Control for an Uncertain Quadrotor UAV Subjected to Disturbances. *ISA Trans.* **2020**, *99*, 290–304. [[CrossRef](#)] [[PubMed](#)]
- Mechali, O.; Xu, L.; Xie, X.; Iqbal, J. Theory and Practice for Autonomous Formation Flight of Quadrotors via Distributed Robust Sliding Mode Control Protocol with Fixed-time Stability Guarantee. *Control Eng. Pract.* **2022**, *123*, 105150. [[CrossRef](#)]
- Labbadi, M.; Cherkaoui, M. Robust Adaptive Backstepping Fast Terminal Sliding Mode Controller for Uncertain Quadrotor UAV. *Aerosp. Sci. Technol.* **2019**, *93*, 105306. [[CrossRef](#)]
- Comert, C.; Kasnakoglu, C. Comparing and Developing PID and Sliding Mode Controllers for Quadrotor. *Int. J. Mech. Eng. Robot. Res.* **2017**, *6*, 194–199. [[CrossRef](#)]
- Elyalaoui, K.; Labbadi, M.; Boubaker, S.; Kamel, S.; Alsubaei, F.S. On Novel Fractional-Order Trajectory Tracking Control of Quadrotors: A Predefined-Time Guarantee Performance Approach. *Mathematics* **2023**, *11*, 3582. [[CrossRef](#)]
- Raffo, G.V.; Ortega, M.G.; Rubio, F. An Integral Predictive/nonlinear H_∞ Control Structure for a Quadrotor Helicopter. *Automatica* **2010**, *46*, 29–39. [[CrossRef](#)]
- Zheng, E.-H.; Xiong, J.-J.; Luo, J.-L. Second Order Sliding Mode Control for a Quadrotor UAV. *ISA Trans.* **2014**, *53*, 1350–1356. [[CrossRef](#)] [[PubMed](#)]
- Tian, B.; Tian, B.; Lu, H.; Zuo, Z.; Zong, Q.; Zhang, Y. Multivariable Finite-time Output Feedback Trajectory Tracking Control of Quadrotor Helicopters. *Int. Robust Nonlinear Control* **2018**, *28*, 281–295. [[CrossRef](#)]
- Xie, W.; Cabecinhas, D.; Cunha, R.; Silvestre, C. Adaptive Backstepping Control of a Quadcopter with Uncertain Vehicle Mass, Moment of Inertia, and Disturbances. *IEEE Trans. Ind. Electron.* **2022**, *69*, 549–559. [[CrossRef](#)]
- Guo, Y.; Ma, B. Global Sliding Mode with Fractional Operators and Application to Control Robot Manipulators. *Int. J. Control* **2019**, *92*, 1497–1510. [[CrossRef](#)]
- Ni, J.; Liu, L.; Liu, C.; Hu, X.; Li, S. Fast Fixed-time Nonsingular Terminal Sliding Mode Control and Its Application to Chaos Suppression in Power System. *Circuits Syst. II Exp. Briefs* **2017**, *64*, 151–155. [[CrossRef](#)]

18. Wang, Z.; Wang, J.; La Scala, M. A Novel Distributed-decentralized Fixed-time Optimal Frequency and Excitation Control Framework in a Nonlinear Network-preserving Power System. *IEEE Trans. Power Syst.* **2021**, *36*, 1285–1297. [[CrossRef](#)]
19. Zeng, T.; Ren, X.; Zhang, Y. Fixed-time Sliding Mode Control and High-gain Nonlinearity Compensation for Dual-motor Driving System. *IEEE Trans. Ind. Inform.* **2020**, *16*, 4090–4098. [[CrossRef](#)]
20. Muñoz-Vázquez, A.J.; Sanchez-Torres, J.D.; Jiménez-Rodríguez, E.; Loukianov, A.G. Predefined-time Robust Stabilization of Robotic Manipulators. *IEEE/ASME Trans. Mechatron.* **2019**, *24*, 2709–2722. [[CrossRef](#)]
21. Muñoz-Vázquez, A.J.; Fernández-Anaya, G.; Sanchez-Torres, J.D.; Meléndez-Vázquez, F. Predefined-time Control of Distributed-order Systems. *Nonlinear Dyn.* **2021**, *103*, 2689–2700. [[CrossRef](#)]
22. Ni, J.; Liu, L.; Tang, Y.; Liu, C. Predefined-time Consensus Tracking of Second-order Multiagent Systems. *IEEE Trans. Syst.* **2021**, *51*, 2550–2560. [[CrossRef](#)]
23. Benaddy, A.; Labbadi, M.; Elyaaloui, K.; Bouzi, M. Fixed-Time Fractional-Order Sliding Mode Control for UAVs under External Disturbances. *Fractal Fract.* **2023**, *7*, 775. [[CrossRef](#)]
24. Muñoz-Vázquez, A.J.; Parra-Vega, V.; Sánchez-Orta, A.; Romero-Galván, G. Fractional PD IAD Error Manifolds for Robust Tracking Control of Robotic Manipulators. *J. Dyn. Syst. Meas. Control* **2019**, *141*, 031006-6. [[CrossRef](#)]
25. Wang, N.; Deng, Q.; Xie, G.; Pan, X. Hybrid Finite-time Trajectory Tracking Control of a Quadrotor. *ISA Trans.* **2019**, *90*, 278–286. [[CrossRef](#)] [[PubMed](#)]
26. Huang, S.; Wang, J.; Xiong, L.; Liu, J.; Li, P.; Wang, Z. Distributed Predefined-Time Fractional-Order Sliding Mode Control for Power System With Prescribed Tracking Performance. *IEEE Trans. Power Syst.* **2022**, *37*, 2233–2246. [[CrossRef](#)]
27. Bhat, S.P.; Bernstein, D.S. Finite-time Stability of Continuous Autonomous Systems. *SIAM J. Control Optim.* **2000**, *38*, 1430–1443. [[CrossRef](#)]
28. Polyakov, A. Nonlinear Feedback Design for Fixed-time Stabilization of Linear Control Systems. *IEEE Trans. Autom. Control* **2012**, *57*, 2106–2110. [[CrossRef](#)]
29. Fraguera, L.; Angulo, M.T.; Moreno, J.A.; Fridman, L. Design of a prescribed convergence time uniform Robust Exact Observer in the presence of measurement noise. In Proceedings of the IEEE 51st IEEE Conference on Decision and Control, Maui, HI, USA, 10–13 December 2012. [[CrossRef](#)]
30. Sanchez-Torres, J.D.; Sanchez-Torres, J.D.; Gómez-Gutiérrez, D.; López, E.; Loukianov, A.G. A Class of Predefined-time Stable Dynamical Systems. *IMA J. Math. Control Inf.* **2018**, *35*, i1–i29. [[CrossRef](#)]
31. Pourmahmood Aghababa, M. A Novel Terminal Sliding Mode Controller for a Class of Non-autonomous Fractional-order Systems. *Nonlinear Dyn.* **2013**, *73*, 679–688. [[CrossRef](#)]
32. Podlubny, I. *Fractional Differential Equations*; Academic Press: New York, NY, USA. Available online: <https://shop.elsevier.com/books/fractional-differential-equations/podlubny/978-0-12-558840-9> (accessed on 1 January 1999).
33. Benaddy, A.; Labbadi, M.; Bouzi, M. Adaptive Nonlinear Controller for the Trajectory Tracking of the Quadrotor with Uncertainties. In Proceedings of the 2020 2nd Global Power, Energy and Communication Conference (GPECOM), Izmir, Turkey, 20–23 October 2020. [[CrossRef](#)]
34. Liang, C.-D.; Ge, M.-F.; Ge, M.-F.; Liu, Z.-W.; Ling, G.; Liu, F.; Liu, F. Predefined-time Formation Tracking Control of Networked Marine Surface Vehicles. *Control Eng. Pract.* **2021**, *107*, 104682. [[CrossRef](#)]
35. Chen, F.; Jiang, R.; Zhang, K.; Jiang, B.; Tao, G. Robust Backstepping Sliding-mode Control and Observer-based Fault Estimation for a Quadrotor UAV. *IEEE Trans. Ind. Electron.* **2016**, *63*, 5044–5056. [[CrossRef](#)]

Disclaimer/Publisher’s Note: The statements, opinions and data contained in all publications are solely those of the individual author(s) and contributor(s) and not of MDPI and/or the editor(s). MDPI and/or the editor(s) disclaim responsibility for any injury to people or property resulting from any ideas, methods, instructions or products referred to in the content.